Biochimica et Biophysica Acta 1840 (2014) 1051–1062

Contents lists available at ScienceDirect

Biochimica et Biophysica Acta

journal homepage: www.elsevier.com/locate/bbagen

Syntheses and characterization of non-bisphosphonate quinoline derivatives as new FPPS inhibitors

Jinggong Liu [a], Weilin Liu [a], Hu Ge [a], Jinbo Gao [b], Qingqing He [a], Lijuan Su [a], Jun Xu [a], Lian-quan Gu [a], Zhi-shu Huang [a], Ding Li [a,*]

[a] School of Pharmaceutical Sciences, Sun Yat-sen University, Guangzhou University City, 132 Waihuan East Road, Guangzhou 510006, P. R. China
[b] Department of Biology and Chemistry, City University of Hong Kong, 83 Tat Chee Avenue, Kowloon, Hong Kong, P. R. China

ARTICLE INFO

Article history:
Received 9 August 2013
Received in revised form 11 October 2013
Accepted 8 November 2013
Available online 15 November 2013

Keywords:
Quinoline derivative
Bisphosphonate
Farnesyl pyrophosphate synthase
Allosteric site
Cancer

ABSTRACT

Background: Farnesyl pyrophosphate synthase (FPPS) is a key regulatory enzyme in the biosynthesis of cholesterol and in the post-translational modification of signaling proteins. It has been reported that non-bisphosphonate FPPS inhibitors targeting its allosteric binding pocket are potentially important for the development of promising anti-cancer drugs.
Methods: The following methods were used: organic syntheses of non-bisphosphonate quinoline derivatives, enzyme inhibition studies, fluorescence titration assays, synergistic effect studies of quinoline derivatives with zoledronate, ITC studies for the binding of FPPS with quinoline derivatives, NMR-based HAP binding assays, molecular modeling studies, fluorescence imaging assay and MTT assays.
Results: We report our syntheses of a series of quinoline derivatives as new FPPS inhibitors possibly targeting the allosteric site of the enzyme. Compound **6b** showed potent inhibition to FPPS without significant hydroxyapatite binding affinity. The compound showed synergistic inhibitory effect with active-site inhibitor zoledronate. ITC experiment confirmed the good binding effect of compound **6b** to FPPS, and further indicated the binding ratio of 1:1. Molecular modeling studies showed that **6b** could possibly bind to the allosteric binding pocket of the enzyme. The fluorescence microscopy indicated that these compounds could get into cancer cells.
Conclusions: Our results showed that quinoline derivative **6b** could become a new lead compound for further optimization for cancer treatment.
General significance: The traditional FPPS active-site inhibitors bisphosphonates show poor membrane permeability to tumor cells, due to their strong polarity. The development of new non-bisphosphonate FPPS inhibitors with good cell membrane permeability is potentially important.

1. Introduction

Bisphosphonates are an important class of drug molecules that are widely used to treat the bone loss associated with osteoporosis [1], Paget's disease [2], hypercalcemia [3], and metastatic bone disease [4]. The main bisphosphonates in clinical use are thought to act primarily by inhibiting the farnesyl diphosphate synthase (FPPS), an important enzyme in the biosynthesis of cholesterol and in the post-translational modification of signaling proteins [5–10]. The inhibition results in decreased prenylation of proteins such as Ras, Rho, Rac, and Rap, and impairment of cell survival signaling pathway [11–13]. However, due to the strong polarity and high hydrophilicity, the bisphosphonate drugs show poor cell-membrane permeability to tumor cells and other non-endocytic cells [5,14]. Several approaches have been taken to optimize the pharmacokinetic properties of bisphosphonates, such as reducing bone affinity with deoxy-bisphosphonates, or reducing the polarity of the compounds by increasing side chain lipophilicity [15–19]. In our previous work, we have developed a new type of nitrogen-containing bisphosphonate analogs with a geranyl group attached to one of phosphate groups showing nanomole inhibition effect to FPPS with our newly developed assay method [20,21].

Recently, Jahnke group has reported a new type of non-bisphosphonate inhibitors identified by fragment-based discovery targeting a new allosteric pocket of FPPS [22], and quinolines and salicylic derivatives have been shown as inhibitors of FPPS. Here, we report our further design and synthesis of another series of quinoline derivatives as new FPPS inhibitors. The combination of quinoline derivative **6b** with zoledronate, an inhibitor targeting active site of FPFS, showed higher inhibition effect than that of one individual inhibitor. Molecular modeling study showed that **6b** can bind well with the

Abbreviations: BPs, bisphosphonates; BSA, bovine serum albumin; DTT, DL-dithiothreitol; FPPS, farnesyl pyrophosphate synthase; HAP, hydroxyapatite; MTT, 3-(4,5-dimethylthiazol-2-yl)-2,5-diphenyl-tetrazolium bromide; Tris, tris(hydroxymethyl)aminomethane

* Corresponding author. Tel./fax: +86 20 3994 3058.
E-mail address: liding@mail.sysu.edu.cn (D. Li).

0304-4165/$ – see front matter © 2013 Elsevier B.V. All rights reserved.
http://dx.doi.org/10.1016/j.bbagen.2013.11.006

allosteric site of the FPPS. The fluorescence microscopy indicated that these quinoline derivatives could get into cancer cells.

2. Materials and methods

2.1. Materials

All the reagents used in the biological assay were analytical pure. Chemical reagents used in the synthesis were of research grade or better and were obtained from commercial sources. Zoledronate was purchased from the Dalian Meilun Biotech Co., Ltd.

2.2. Organic syntheses of quinoline derivatives

^{1}H and ^{13}C NMR spectra were recorded using TMS as the internal standard in DMSO-d_6, CD_3COCD_3 or $CDCl_3$ with a Bruker BioSpin GmbH spectrometer at 400 MHz; Mass spectra (MS) were recorded on a Shimadzu LCMS-2010A instrument with an ESI-ACPI mass selective detector, and high resolution mass spectra (HRMS) were recorded on Shimadzu LCMS-IT-TOF. Flash column chromatography was performed with silica gel (200–300 mesh) purchased from Qingdao Haiyang Chemical Co. Ltd. Organic syntheses of bisphosphonate derivatives were shown in Schemes 1–4.

2.2.1. General procedures for the preparation of intermediates 1, 2, and 3

The syntheses of intermediates were as those reported before [23,24] with some modifications. Aniline (100 mmol, 9.31 g) or 1-naphthylamine (100 mmol, 14.3 g) and ethyl acetoacetate (100 mmol, 13.0 g) or ethyl 4-chloroacetoacetate (100 mmol, 16.4 g) in 100 mL PPA were heated at 130 °C for 1 h. After cooling and neutralization, $POCl_3$ was added to the solid product, and heated under reflux at 100 °C for 3 h. The mixtures were cooled and poured into ice-water mixture. After neutralization, it was filtered and dried to give the intermediates **1**, **2** and **3**, which were used directly for the following reaction without further purification.

2.2.2. Synthesis of methyl 2-((2-(chloromethyl)quinolin-4-yl)amino) benzoate (4a) and 2-((2-(chloromethyl)quinolin-4-yl)amino)benzoic acid (4b)

The synthesis of **4a** was similar to that reported previously [25]. Intermediate **1** (10 mmol, 2.11 g) was added to a solution of methyl 2-aminobenzoate (10 mmol, 1.51 g) in ethanol, followed by two drops of concentrated hydrochloric acid. The mixture was heated under reflux at 80 °C for 5 h. After evaporation of the solvent, the crude product was purified with gel chromatography to give compound **4a** as a white solid (2.62 g, 80%). ^{1}H NMR (400 MHz, $CDCl_3$) δ 10.57 (s, 1H), 8.14 (d, J = 8.0 Hz, 1H), 8.09 (dd, J = 8.0, 1.6 Hz, 1H), 8.05 (d, J = 8.4 Hz, 1H), 7.76 − 7.69 (m, 2H), 7.63 (s, 1H), 7.61 − 7.52 (m, 2H), 7.05 − 7.01 (m, 1H), 4.76 (s, 3H), 3.96 (s, 3H); ^{13}C NMR (100 MHz, $CDCl_3$) δ 168.9, 157.2, 148.7, 146.3, 144.3, 134.2, 131.9, 130.1, 129.7, 126.5, 121.0, 120.8, 120.7, 117.6, 115., 104.3, 52.3, 47.7; ESI-HRMS m/z: calcd for $C_{18}H_{15}N_2O_2Cl$ $[M-H]^-$ 325.0749, found 325.0747.

48 mg LiOH (dissolved in 0.1 mL H_2O) was added to a solution of **4a** (1 mmol, 0.326 g) in THF/CH_3OH (2.5 mL, 2.5 mL), and the mixture was heated under reflux for 3 h. After cooling and neutralization with 1 N HCl, the solution was filtered and dried to give a white solid **4b** (296 mg, 94.8%). ^{1}H NMR (400 MHz, DMSO) δ 12.80 (s, 1H), 9.47–9.45 (m, 1H), 9.17 (s, 1H), 8.12 (d, J = 7.2 Hz, 3H), 7.90 − 7.88 (m, 2H), 7.86 − 7.80 (m, 2H), 7.42 − 7.38 (m, 1H), 6.83 (d, J = 8.4 Hz, 1H), 6.63 (t, J = 7.4 Hz, 1H), 4.84 (s, 3H); ^{13}C NMR (100 MHz, DMSO) δ 169.9, 157.3, 150.1, 145.8, 141.6, 134.5, 133.4, 131.8, 130.2, 129.0, 128.7, 128.1, 127.7, 124.6, 122.3, 120.5, 120.3, 114.7, 111.8, 110.8, 47.6; ESI-HRMS m/z: calcd for $C_{17}H_{13}ClN_2O_2$ $[M-H]^-$ 312.0756, found 312.0759.

2.2.3. Synthesis of ethyl 2-((4-chloroquinolin-2-yl)methoxy)benzoate (5a) and 2-((4-chloroquinolin-2-yl)methoxy)benzoic acid (5b)

Intermediate **1** (10 mmol, 2.11 g) was dissolved in 50 mL CH_3CN. After the addition of ethyl 2-hydroxybenzoate (11 mmol, 1.83 g), followed by K_2CO_3 (10 mmol, 1.38 g), the mixture was heated at 90 °C for 5 h. The solution was poured into water, and filtered to give a white solid **5a** (2.32 g, 68%). ^{1}H NMR (400 MHz, $CDCl_3$) δ 8.25 (d, J = 9.2 Hz, 1H), 8.10 (d, J = 10.0 Hz, 2H), 7.88 (dd, J = 7.8, 1.8 Hz, 1H), 7.82 − 7.78 (m, 1H), 7.67 − 7.63 (m, 1H), 7.46 (m, 1H), 7.05 (dd, J = 16.0, 8.0 Hz, 2H), 5.44 (s, 2H), 4.46 (q, J = 7.2 Hz, 2H), 1.44 (t, J = 7.2 Hz, 3H); ^{13}C NMR (100 MHz, $CDCl_3$) δ 181.1, 166.3, 157.8 157.5, 148.2, 143.7, 133.5, 132.0, 130.6, 129.2, 127.4, 125.9, 124.2, 121.11, 121.05, 119.4, 113.5, 71.2, 61.1, 14.4; ESI-HRMS m/z: calcd for $C_{19}H_{16}NO_3Cl$ $[M + Na]^+$ 364.0711, found 364.0703.

The hydrolysis procedure for **5a** was the same as that for **4a**, and the desired product **5b** was obtained as a white solid. ^{1}H NMR (400 MHz, DMSO) δ 12.92 (s, 1H), 8.23 (d, J = 8.4 Hz, 1H), 8.12–8.09 (m, 2H), 7.91 (t, J = 7.8 Hz, 1H), 7.80 − 7.74 (m, 2H), 7.56 − 7.51 (m, 1H), 7.29 (d, J = 8.0 Hz, 1H), 7.07 (t, J = 7.4 Hz, 1H), 5.47 (s, 3H);

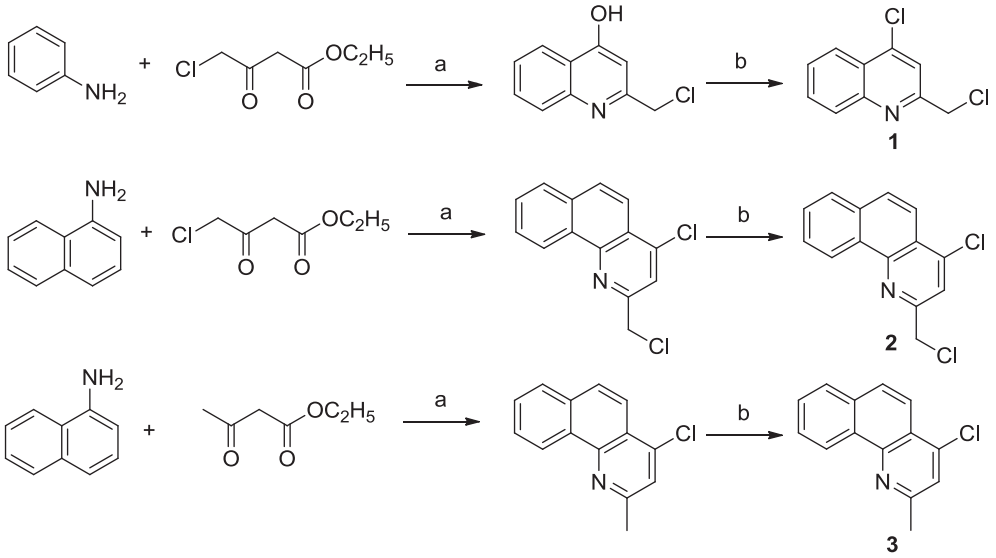

Scheme 1. Syntheses of the intermediates **1**, **2** and **3**. Reagents and conditions: (a) PPA, 130 °C, 1 h; (b) $POCl_3$, 100 °C, 3 h.

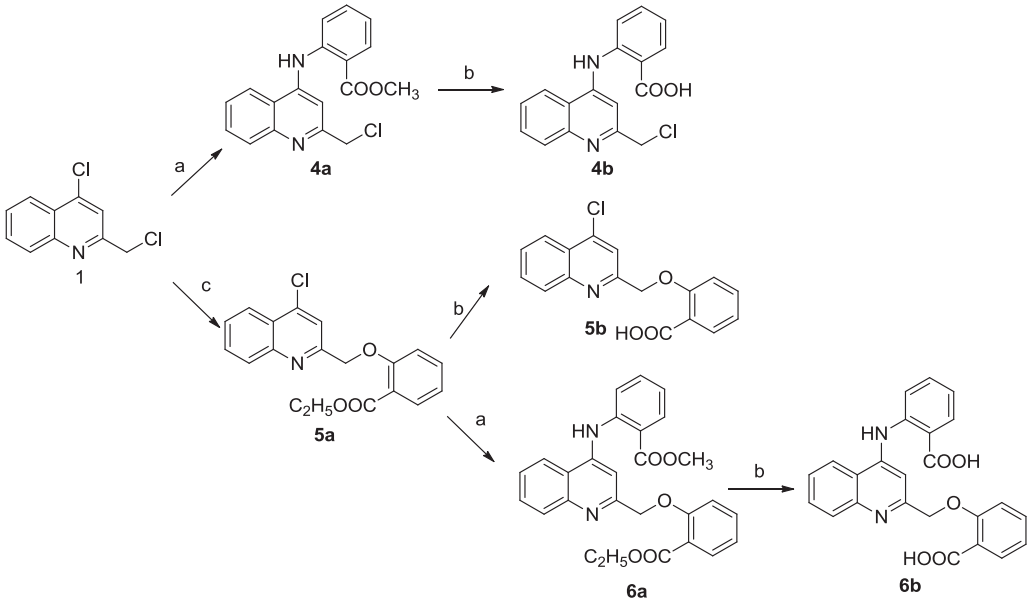

Scheme 2. Syntheses of **4a**–**6b**. Reagents and conditions: (a) methyl 2-aminobenzoate, C_2H_5OH, conc. HCl, 5 h; (b) THF/CH_3OH, LiOH, 3 h; (c) ethyl 2-hydroxybenzoate, K_2CO_3, CH_3CN, 90 °C, 5 h.

^{13}C NMR (100 MHz, DMSO) δ 167.1, 158.1, 156.8, 147.7, 142.1, 133.3, 131.1, 131.0, 129.0, 128.0, 124.8, 123.6, 121.6, 120.9, 119.4, 114.1, 70.5; ESI-HRMS m/z: calcd for $C_{17}H_{12}NO_3Cl$ [M-H]$^-$ 312.0433, found 312.0433.

*2.2.4. Synthesis of ethyl 2-((4-((2-(methoxycarbonyl)phenyl)amino) quinolin-2-yl)methoxy)benzoate (**6a**) and 2-((2-((2-carboxyphenoxy) methyl)quinolin-4-yl)amino)benzoic acid (**6b**)*

Compound **5a** was reacted with methyl 2-aminobenzoate following the procedure for the synthesis of **4a** to give the desired product **6a**, and the hydrolysis procedure for **6a** was the same as that for **4a**. **6a**: ^{1}H NMR (400 MHz, $CDCl_3$) δ 10.65 (s, 1H), 8.16 (d, J = 8.0 Hz, 1H), 8.07–8.03 (m, 2H), 7.91 (s, 1H), 7.84 (dd, J = 7.8, 1.8 Hz, 1H), 7.73 (m, 1H), 7.62 (d, J = 8.0 Hz, 1H), 7.59 − 7.56 (m, 1H), 7.49 − 7.45 (m, 1H), 7.45 − 7.40 (m, 1H), 7.07 (d, J = 8.4 Hz, 1H), 6.99 (td, J = 8.6, 0.8 Hz, 2H), 5.43 (s, 2H), 4.24 (q, J = 7.2 Hz, 2H), 3.95 (s, 3H), 1.25 (t, J = 7.2 Hz, 3H); ^{13}C NMR (100 MHz, $CDCl_3$) δ 169.0, 166.0, 158.1, 157.6, 145.9, 144.3, 134.5, 133.4, 131.6, 131.6, 129.8, 129.2, 126.0, 121.1, 120.9, 120.8, 120.6, 120.3, 117.7, 115.4, 113.6, 103.1, 71.4, 60.7, 52.2, 14.2; ESI-HRMS m/z: calcd for $C_{27}H_{24}N_2O_5$ [M + H]$^+$ 457.1758, found 457.1729.

6b: ^{1}H NMR (400 MHz, DMSO) δ 10.99 (s, 1H), 8.22 (d, J = 8.0 Hz, 1H), 8.05 (d, J = 8.0 Hz, 1H), 7.97 (d, J = 8.4 Hz, 1H), 7.83 (t, J = 7.4 Hz, 1H), 7.72 − 7.65 (m, 3H), 7.61 (d, J = 3.2 Hz, 2H), 7.50 − 7.46 (m, 2H), 7.27 (d, J = 8.4 Hz, 1H), 7.20 − 7.16 (m, 1H), 7.05 (t, J = 7.4 Hz, 1H), 5.49 (s, 3H); ^{13}C NMR (100 MHz, DMSO) δ 174.7, 172.3, 162.4, 161.8, 152.3, 151.5, 147.4, 139.2, 138.3, 137.1, 136.2, 135.9, 132.4, 1315, 127.6, 127.5, 126.4, 126.4, 124.8, 124.8, 124.3, 119.8, 106.0, 75.5; ESI-HRMS m/z: calcd for $C_{24}H_{18}N_2O_5$ [M + H]$^+$ 415.1288, found 415.1269.

*2.2.5. Synthesis of ethyl 2-((4-chlorobenzo[h]quinolin-2-yl)methoxy) benzoate (**7a**) and 2-((4-chlorobenzo[h]quinolin-2-yl)methoxy)benzoic acid (**7b**)*

Intermediate **2** was reacted with ethyl 2-hydroxybenzoate following the procedure described in Section 2.2.3, and the desired products **7a** and **7b** were obtained as white solids. **7a**: ^{1}H NMR (400 MHz, $CDCl_3$) δ 9.34 (d, J = 8.0 Hz, 1H), 8.13 (d, J = 11.2 Hz, 2H), 7.95 − 7.90 (m, 3H), 7.78 − 7.72 (m, 2H), 7.49 − 7.45 (m, 1H), 7.14 (d, J = 8.4 Hz, 1H), 7.05 (t, J = 7.2 Hz, 1H), 5.56 (s, 3H), 4.47 (q, J = 7.2 Hz, 2H), 1.45 (t, J = 7.2 Hz, 3H); ^{13}C NMR (100 MHz, $CDCl_3$) δ 166.5, 157.6, 156.3, 146.8, 143.4, 133.8, 133.5, 132.0, 130.9, 128.8, 128.6, 127.9, 127.4, 125.0, 123.6, 121.1, 121.0, 120.9, 120.0, 113.6, 71.3, 61.1, 14.5; ESI-HRMS m/z: calcd for $C_{23}H_{18}NO_3Cl$ [M + H]$^+$ 392.1048, found 392.1041.

7b: ^{1}H NMR (400 MHz, DMSO) δ 9.18 (dd, J = 8.0, 4.0 Hz, 1H), 8.27 (s, 1H), 8.09 (s, 3H), 7.82 (dd, J = 6.2, 3.4 Hz, 2H), 7.64 (d, J = 6.4 Hz, 1H), 7.42 (t, J = 7.6 Hz, 1H), 7.24 (d, J = 8.0 Hz, 1H), 7.01 (t, J = 7.4 Hz, 1H), 5.53 (s, 2H); ^{13}C NMR (100 MHz, DMSO) δ 168.2, 157.2, 156.2, 145.9, 142.0, 133.3, 131.6, 130.4, 130.0, 129.0, 128.8 128.1, 127.6, 124.3, 122.6, 120.7, 120.2, 113.9, 70.6; ESI-HRMS m/z: calcd for $C_{21}H_{14}NOCl$ [M-H]$^-$ 362.0589, found 362.0603.

*2.2.6. Synthesis of methyl 4-chloro-2-((4-((4-methoxyphenyl)amino) benzo[h]quinolin-2-yl)methoxy)benzoate (**8a**) and 4-chloro-2-((4-((4-methoxyphenyl)amino)benzo[h]quinolin-2-yl)methoxy)benzoic acid (**8b**)*

Intermediate **2** was reacted with methyl 4-chloro-2-hydroxybenzoate following the procedure described in Section 2.2.3, and the resulting product methyl 4-chloro-2-((4-chlorobenzo[h]quinolin-2-yl)methoxy) benzoate was then reacted with 4-methoxyaniline following the procedure described in Section 2.2.2, to give the desired bright yellow product **8a** and yellow product **8b**. **8a**: ^{1}H NMR (400 MHz, $CDCl_3$) δ

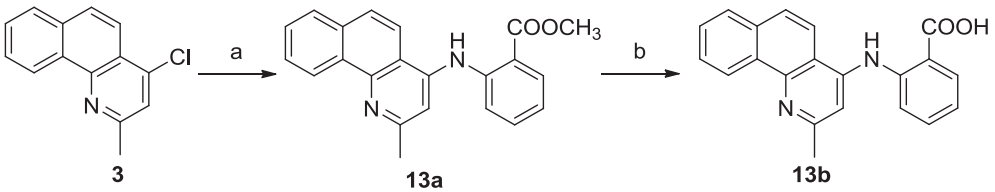

Scheme 3. Syntheses of **13a** and **13b**. Reagents and conditions: (a) methyl 2-aminobenzoate, C_2H_5OH, conc. HCl, 5 h; (b) THF/CH_3OH, LiOH, 3 h.

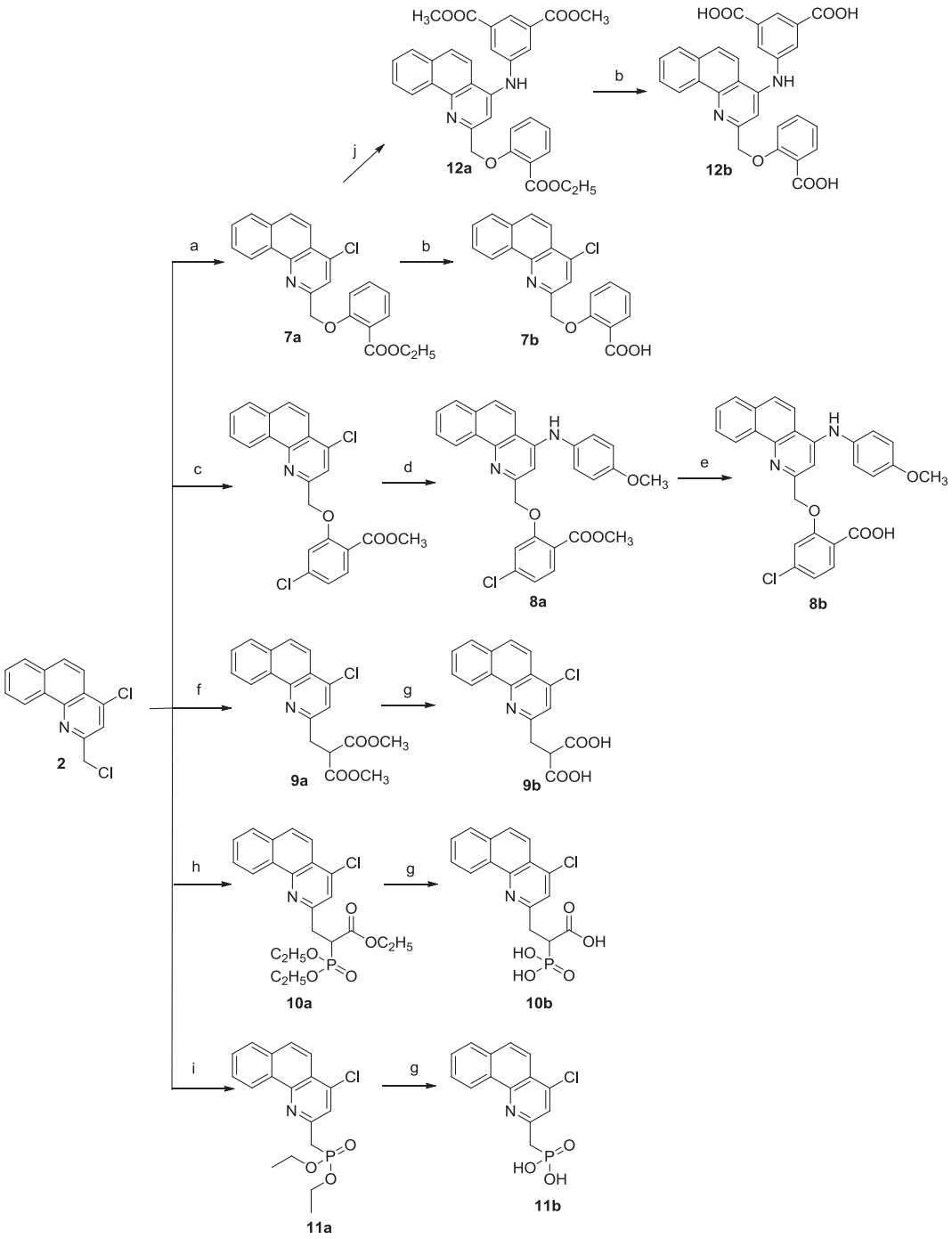

Scheme 4. Syntheses of **7a–12b**. Reagents and conditions: (a) ethyl 2-hydroxybenzoate, K_2CO_3, CH_3CN, 90 °C, 5 h; (b) THF/CH_3OH, LiOH, 3 h; (c) methyl 4-chloro-2-hydroxybenzoate, K_2CO_3, CH_3CN, 90 °C, 5 h; (d,e) 4-methoxyaniline, C_2H_5OH, conc. HCl, 5 h; (f) dimethyl malonate, NaH, THF, 0 °C, 10 h; (g) conc. HCl, 150 °C, 24 h; (h) ethyl 2-(diethoxyphosphoryl)acetate, NaH, THF, 0 °C, 10 h; (i) triethyl phosphate; (j) dimethyl 5-aminoisophthalate, C_2H_5OH, conc. HCl, 5 h.

9.30 (d, J = 8.0 Hz, 1H), 7.86 (d, J = 7.2 Hz, 1H), 7.76 (q, J = 10.8 Hz, 3H), 7.72 − 7.63 (m, 2H), 7.29 (s, 1H), 7.23 − 7.19 (m, 3H), 6.95 (dd, J = 13.0, 9.4 Hz, 3H), 6.67 (s, 1H), 3.83 (s, 3H), 3.68 (s, 3H); ^{13}C NMR (100 MHz, $CDCl_3$) δ 174.8, 165.7, 158.7, 157.2, 139.4, 133.6, 132.8, 128.0, 127.6, 126.9, 125.3, 125.0, 120.8, 117.2, 115.2, 114.7, 114.5, 114.2, 101.0, 55.5, 51.8; ESI-HRMS m/z: calcd for $C_{29}H_{23}ClN_2O_4$ $[M-H]^-$ 498.1357, found 498.1346.

8b: ^{1}H NMR (400 MHz, DMSO) δ 10.40 (s, 1H), 9.27 (s, 1H), 8.54 (d, J = 8.5 Hz, 1H), 8.17 (d, J = 4.8 Hz, 1H), 8.12 (d, J = 8.8 Hz, 1H), 7.91 − 7.87 (m, 2H), 7.77 (d, J = 8.4 Hz, 1H), 7.39 (d, J = 1.6 Hz, 1H), 7.31 (s, 1H), 7.29 (s, 1H), 7.17 (dd, J = 8.4, 1.2 Hz, 1H), 7.09 − 7.04 (m, 3H), 5.63 (s, 3H), 3.82 (s, 3H); ESI-HRMS m/z: calcd for $C_{28}H_{21}N_2O_4Cl$ $[M-H]^-$ 483.1117, found 483.1127.

*2.2.7. Synthesis of dimethyl 2-((4-chlorobenzo[h]quinolin-2-yl)methyl) malonate (**9a**) and 2-((4-chlorobenzo[h]quinolin-2-yl)methyl)malonic acid (**9b**)*

Sodium hydride (120 mg, 80%) was added to a solution of dimethyl malonate (2 mmol, 0.264 g) dissolved in newly distilled THF at 0 °C. After stirring for 30 min, a solution of intermediate **2** dissolved in distilled THF was added dropwise to the mixture. After stirring for 10 h at 0 °C, the mixture was filtered, the solvent was removed, and

the crude product was purified using silica gel chromatography to give the desired brown product **9a** with a yield of 62%. ^{1}H NMR (400 MHz, $CDCl_3$) δ 9.28 − 9.25 (m, 1H), 8.07 (d, J = 9.2 Hz, 1H), 7.90 (dd, J = 6.8, 2.4 Hz, 1H), 7.86 (d, J = 9.2 Hz, 1H), 7.75 − 7.69 (m, 2H), 7.53 (s, 1H), 4.54 (t, J = 7.6 Hz, 1H), 3.79 (s, 6H), 3.71 (d, J = 7.6 Hz, 2H); ^{13}C NMR (100 MHz, $CDCl_3$) δ 169.8, 156.4, 146.7, 142.6, 133.8, 131.1, 128.7, 128.2, 127.8, 127.3, 125.1, 122.9, 121.8, 120.8, 52.7, 49.8, 36.3; ESI-HRMS m/z: calcd for $C_{19}H_{16}NO_4Cl$ $[M + H]^+$ 358.0841, found 358.0861.

2 mL concentrated hydrochloric acid was directly added to **9a** (1 mmol, 0.357 g) and heated at 150 °C for 24 h. The solution was neutralized with 1 N NaOH. After filtration and drying, a brown product **9b** was obtained with nearly 100% yield. **9b**: ^{1}H NMR (400 MHz, Acetone) δ 9.35 − 9.32 (m, 1H), 8.11 (d, J = 9.2 Hz, 1H), 8.03 (t, J = 8.6 Hz, 2H), 7.77 (m, 3H), 4.43 (t, J = 7.2 Hz, 1H), 3.72 (d, J = 7.0 Hz, 3H); ^{13}C NMR (100 MHz, Acetone) δ 171.0, 159.0, 147.5, 142.8, 134.8, 131.9, 129.7, 129.3, 129.1 128.8, 128.3, 126.1 123.3, 123.1, 121.3, 50.3, 37.2; ESI-HRMS m/z: calcd for $C_{17}H_{12}NO_4Cl$ $[M-H]^-$ 328.0382, found 328.0368.

2.2.8. Synthesis of ethyl 3-(4-chlorobenzo[h]quinolin-2-yl)-2-(diethoxyphosphoryl)propanoate (**10a**) and 3-(4-chlorobenzo[h]quinolin-2-yl)-2-phosphonopropanoic acid (**10b**)

Intermediate **2** was reacted with ethyl 2-(diethoxyphosphoryl) acetate following the procedure described in Section 2.2.7. The desired product **10a** was obtained as a dark brown solid, and **10b** was obtained by hydrolyzing **10a** with concentrated hydrochloric acid directly. **10a**: ^{1}H NMR (400 MHz, $CDCl_3$) δ 9.26 (dd, J = 6.0, 2.8 Hz, 1H), 8.08 (d, J = 9.2 Hz, 1H), 7.92 − 7.90 (m, 1H), 7.85 (d, J = 9.2 Hz, 1H), 7.71 (m, 2H), 7.52 (s, 1H), 4.31 − 4.18 (m, 6H), 4.17 − 4.12 (m, 1H), 3.81 (m, 1H), 3.57 (m, 1H), 1.39 (dt, J = 10.8, 7.0 Hz, 6H), 1.23 (t, J = 7.2 Hz, 3H); ^{13}C NMR (100 MHz, $CDCl_3$) δ 169.0, 156.8, 146.7, 142.4, 133.7, 131.2, 128.6, 128.1, 127.7, 127.2, 125.2, 122.8, 121.8, 120.8, 62.9, 61.5, 44.1, 42.8, 34.5, 16.4, 14.1; ESI-HRMS m/z: calcd for $C_{22}H_{25}NO_5PCl$ $[M + H]^+$ 450.1232, found 450.1237.

10b: ^{1}H NMR (400 MHz, DMSO) δ 9.22 (d, J = 4.8 Hz, 1H), 8.03 (s, 3H), 7.78 (s, 3H), 3.75 (d, J = 8.0 Hz, 1H), 3.69 − 3.63 (m, 2H); ESI-HRMS m/z: calcd for $C_{17}H_{12}NO_4Cl$ $[M-H]^-$ 364.0147, found 364.0160.

2.2.9. Synthesis of diethyl ((4-chlorobenzo[h]quinolin-2-yl)methyl) phosphonate (**11a**) and ((4-chlorobenzo[h]quinolin-2-yl)methyl) phosphonic acid (**11b**)

Intermediate **2** was reacted with triethyl phosphate following the procedure described in Section 2.2.7, and the desired products **11a** and **11b** were obtained as brown solids. **11a**: ^{1}H NMR (400 MHz, $CDCl_3$) δ 9.27 (d, J = 8.0 Hz, 1H), 8.39 (s, 1H), 8.05 (s, 2H), 7.86 (d, J = 8.8 Hz, 1H), 7.79 (d, J = 6.0 Hz, 1H), 7.72 − 7.65 (m, 4H), 7.63 (s, 1H), 7.44 − 7.40 (m, 1H), 7.09 (d, J = 8.4 Hz, 1H), 6.98 (t, J = 7.4 Hz, 1H), 6.86 (s, 1H), 4.13 (q, J = 7.2 Hz, 2H), 3.90 (s, 6H), 1.22 (t, J = 7.2 Hz, 3H); ESI-HRMS m/z: calcd for $C_{18}H_{19}NO_3PCl$ $[M + H]^+$ 364.0864, found 364.0851.

11b: ^{1}H NMR (400 MHz, DMSO) δ 9.21 (s, 1H), 8.08 (s, 3H), 7.79 (m, 3H), 3.55 (s, 1H), 3.49 (s, 1H); ^{13}C NMR (100 MHz, DMSO) δ 154.8, 146.1, 140.8, 133.2, 130.2, 128.9, 128.4, 128.0, 127.4, 124.5, 122.8, 121.7, 120.2, 38.7; ESI-HRMS m/z: calcd for $C_{14}H_{11}NO_3PCl$ $[M-H]^-$ 308.0238, found 308.0221.

2.2.10. Synthesis of dimethyl 5-((2-((2-(ethoxycarbonyl)phenoxy)methyl) benzo[h]quinolin-4-yl)amino)isophthalate (**12a**) and 5-((2-((2-carboxyphenoxy)methyl)benzo[h]quinolin-4-yl)amino)isophthalic acid (**12b**)

Compound **7a** was reacted with dimethyl 5-aminoisophthalate following the procedure described in Section 2.2.2, and the desired products **12a** and **12b** were obtained as yellow and brown solid, respectively. **12a**: ^{1}H NMR (400 MHz, $CDCl_3$) δ 9.27 (d, J = 8.0 Hz, 1H), 8.39 (s, 1H), 8.05 (s, 2H), 7.86 (d, J = 8.8 Hz, 1H), 7.79 (d, J = 6.0 Hz, 1H), 7.72 − 7.65 (m, 4H), 7.63 (s, 1H), 7.44 − 7.40 (m, 1H), 7.09 (d, J = 8.4 Hz, 1H), 6.98 (t, J = 7.4 Hz, 1H), 6.86 (s, 1H), 4.13 (q, J = 7.2 Hz, 2H), 3.90 (s, 6H), 1.22 (t, J = 7.2 Hz, 3H); ^{13}C NMR (100 MHz, $CDCl_3$) δ 165.9, 158.0, 141.8, 133.4, 131.7, 130.9, 128.8, 128.1, 127.8, 126.9, 126.2, 125.5, 125.0, 120.4, 117.9, 116.4, 113.5, 103.8, 71.5, 60.7, 52.4, 14.2; ESI-HRMS m/z: calcd for $C_{33}H_{28}N_2O_7$ $[M-H]^-$ 563.1824, found 563.1842.

12b: ^{1}H NMR (400 MHz, DMSO) δ 9.33 (d, J = 8.8 Hz, 1H), 8.55 (d, J = 9.2 Hz, 1H), 8.40 (s, 1H), 8.21 (m, 2H), 8.16 (s, 2H), 7.97 − 7.90 (m, 2H), 7.71 (dd, J = 7.6 Hz, 1.5 Hz, 1H), 7.57 − 7.50 (m, 1H), 7.43 (s, 1H), 7.25 (d, J = 8.3 Hz, 1H), 7.07 (t, J = 7.6 Hz, 1H); ^{13}C NMR (100 MHz, DMSO) δ 166.6, 165.9, 156.3, 153.9, 152.2, 138.6, 134.2, 133.3, 132.9 131.3, 130.3, 129.2, 128.7, 128.0, 127.6, 124.0, 121.5, 121.4, 119.3, 114.8, 114.1, 101.2, 66.7; ESI-HRMS m/z: calcd for $C_{29}H_{20}N_2O_7$ $[M + H]^+$ 509.1343, found 509.1338.

2.2.11. Synthesis of methyl 2-(2-methylbenzo[h]quinolin-4-ylamino) benzoate (**13a**) and 2-((2-methylbenzo[h]quinolin-4-yl)amino)benzoic acid (**13b**)

Intermediate **3** was reacted with methyl 2-aminobenzoate following the procedure described in Section 2.2.2, and the desired products **13a** and **13b** were obtained as white solids. **13a**: ^{1}H NMR (400 MHz, $CDCl_3$) δ 10.36 (s, 1H), 9.34 (d, J = 7.2 Hz, 1H), 8.08 (dd, J = 8.0, 1.6 Hz, 1H), 7.99 (d, J = 9.2 Hz, 1H), 7.89 (d, J = 8.0 Hz, 1H), 7.78 (d, J = 9.2 Hz, 1H), 7.72 − 7.65 (m, 2H), 7.59 (d, J = 8.0 Hz, 1H), 7.48 (d, J = 7.2 Hz, 1H), 7.45 (s, 1H), 6.95 (t, J = 7.4 Hz, 1H), 3.96 (s, 3H), 2.77 (s, 3H); ^{13}C NMR (100 MHz, $CDCl_3$) δ 169.0, 158.0, 147.4, 145.4, 145.2, 134.1, 133.7 131.8, 131.6, 127.9, 127.6, 126.8, 126.2, 124.9, 119.7, 118.6, 117.3, 116.8, 114.8, 108.7, 52.2, 25.8; ESI-HRMS m/z: calcd for $C_{22}H_{18}N_2O_2$ $[M + H]^+$ 343.1441, found 343.1441.

13b: ^{1}H NMR (400 MHz, DMSO) δ 13.63 (s, 1H), 10.85 (s, 1H), 9.38 (m, 1H), 8.49 (d, J = 9.2 Hz, 1H), 8.21 (dd, J = 9.2, 4.8 Hz, 2H), 8.11 (dd, J = 8.0, 1.2 Hz, 1H), 7.96 − 7.91 (m, 2H), 7.80 (td, J = 7.6, 1.2 Hz, 1H), 7.67 (d, J = 8.0 Hz, 1H), 7.56 (t, J = 7.2 Hz, 1H), 6.80 (s, 1H), 2.76 (s, 3H); ^{13}C NMR (101 MHz, DMSO) δ 167.1, 154.0, 137.5, 137.1, 134.2, 133.8, 131.8, 130.2, 128.0, 127.9, 127.5, 127.5, 127.1, 126.7, 124.3, 122.9, 118.5, 102.8, 20.1; ESI-HRMS m/z: calcd for $C_{21}H_{16}N_2O_2$ $[M + H]^+$ 329.1285, found 329.1273.

2.3. The enzyme inhibition studies

The enzyme inhibition studies were performed in flat bottom, 96-well plates using our newly developed non-radioactive methods. 100 ng of pure FPPS was incubated with or without inhibitor for 10 min in a final volume of 100 μL buffer, containing 50 mM Tris, pH 7.5, 2 mM $MgCl_2$, 1 mM DTT, 5 mg/mL BSA, and 100 μU/μL of inorganic pyrophosphatase in each well. Then, the substrates were added to start the reaction. Assays were terminated by the addition of 10 μL of 2.5% ammonium molybdate reagent (in 5 N H_2SO_4), 10 μL of 0.5 M 2-mercaptoethanol and 5 μL of Eikonogen reagent (0.25 g of sodium sulfite and 14.7 g of meta-bisulfite dissolved in 100 mL water). The mixtures in plates were incubated with gentle mixing on a plate shaker for 20 min. The absorbance was measured at 830 nm using a Microplate Reader. IC_{50} was determined by a curve fitting of relative activity versus inhibitor concentration using GraphPad Prism 5 Software.

2.4. Fluorescence titration assay

Fluorescence titration assay was performed to evaluate the binding affinity of these compounds to FPPS. The assay was carried out in 50 mM Tris buffer, pH 7.4, 5% glycerol, and 5 mM β-mercaptoethanol. The excitation wavelength used in these experiments was 279 nm. Emission spectra were scanned from 300 to 600 nm, with a 5 nm slit width. For data analysis, the values measured for bound probe at the

Table 1
The IC_{50} and K_d values for inhibition of FPPS by the compounds.

Compound																				
	Zoledronate	**4a**	**4b**	**5a**	**5b**	**6a**	**6b**	**7a**	**7b**	**8a**	**8b**	**9a**	**9b**	**10a**	**10b**	**11a**	**11b**	**12a**	**12b**	**13a**	**13b**
IC_{50} (μM)	0.2	4.10	3.85	4.87	28.6	5.42	3.46	3.51	3.75	7.86	4.28	4.44	10.4	11.6	3.93	13.8	7.92	13.7	5.27	13.3	8.57
K_d (μM)	9	38.4	20.8	31.8	16.5	12.4	5.78	18.8	15.1	15.6	27.5	27.2	8.24	49.0	14.2	18.2	38.6	20.3	16.5	23.0	15.0

fluorescent emission peak of 538–540 nm were corrected for free compounds/buffer and for any scattering occurred. These corrected fluorescence enhancement data or reduced date were used to plot against concentrations of compounds, and analyzed by nonlinear regression to yield dissociation constants (K_d) and extrapolated maximum fluorescence intensity (Fmax). K_d values were estimated by fitting the titration data to the equation $Y = [F_{max}(X)] / [K_d + (X)]$.

2.5. The combination effect study of quinoline derivatives with zoledronate

The combination effect study of quinoline derivatives with zoledronate was performed using the same enzyme inhibition assay. The FPPS was incubated with zoledronate alone or with varying concentrations of quinoline derivatives. The IC_{50} values for zoledronate alone or zoledronate with different concentrations of quinoline derivatives were calculated for the analyses of the combination effect of these two types of compounds. The CompuSyn software [26,27] was used to score the combination effect.

2.6. ITC study for the binding of quinoline derivatives with FPPS

ITC measurements were performed on a VP-ITC calorimeter. The protein was dialyzed extensively against the buffer solution (50 mM HEPES, pH 7.5, 25 mM NaCl, 2 mM DTT), and the ligand was dissolved in the dialysis buffer. Calorimetric titrations were carried out at 25 °C. A typical titration involved 25–30 injections of each ligand (4–10 μL aliquot per injection) at 5-min intervals into the sample cell containing the protein solution. The titration cell was stirred continuously at 307 r.p.m. The heat of the ligand dilution in the buffer alone was subtracted from the titration data for each compound. The data were analyzed to determine binding stoichiometry (N), binding affinity (K_a) and thermodynamic parameters of the reaction using Origin software (OriginLab 7.0).

2.7. NMR-based HAP binding assay

HAP binding assay was performed on a 400 MHz Bruker DRX spectrometer. Solutions (1.0 mL) of quinoline derivatives (50 mM in aqueous buffer containing 50 mM Tris pH 7.5, and 10% D_2O) were divided into two aliquots. One aliquot was incubated with HAP (2.0 mg) for 5 min, centrifuged, and measured by using NMR. The other aliquot was treated identically, but not mixed with HAP.

2.8. Molecular modeling study

To investigate the interacting mode between our synthetic compounds and FPPS (PDB code: 3N6K), a molecular modeling study utilizing the docking module named CDOCKER in Discovery Studio 2.5 (DS 2.5, Accelrys, Inc.) was carried out. The docked poses were clustered and four ligand poses were selected as the starting pose for further MD studies. MD simulation parameter files were prepared for each ligand-receptor complex using LEaP in AMBER 12. The parameters for ligands were adopted from the General Amber Force Field (GAFF), while AMBERff12SB force field was applied for the receptors. Based on the electrostatic potential (ESP) calculations at the ab initio HF/6-31G* level, the partial atomic charges of ligands were calculated by using the restricted electrostatic potential (RESP) fitting protocol implemented in the Antechamber module of the AMBER 12 package. The complexes were neutralized by adding sodium/chlorine counter ions, and solvated in an octahedral box of TIP3P water molecules with solvent layers 10 Å between the box edges and solute surface.

```
  1 MNGDQKLDVHNQEKQNFIQHFSQIVKVLTEDELGHPEKGDAITRIKEVLE  50
 51 YNTVGGKYNRGLTVVQTFQELVEPRKQDAESLQRALTVGWCVELLQAFFL 100
101 VLDDIMDSSHTRRGQICWYQKPGIGLDAINDALLLEAAIYRLLKFYCREQ 150
151 PYYLNLLELFLQSSYQTEIGQTLDLITAPQGQVDLGRYTEKRYKSIVKYK 200
201 TAFYSFYLPIAAAMYMAGIDGEKEHANALKILLEMGEFFQIQDDYLDLFG 250
251 DPSVTGKVGTDIQDNKCSWLVVQCLLRATPQQRQILEENYGQKDPEKVAR 300
301 VKALYEELDLRSVFFKYEEDSYNRLKSLIEQCSAPLPPSIFLELANKIYK 350
351 RRK
```

Fig. 1. The amino acid sequence of rat FPPS (accession code: EDM00670). Rat FPPS contains many tyrosines, tryptophans, and phenylalanines, such as Tyr10, Tyr58, Tyr204, Tyr349, Phe206, Phe239, which let the enzyme have fluorescence.

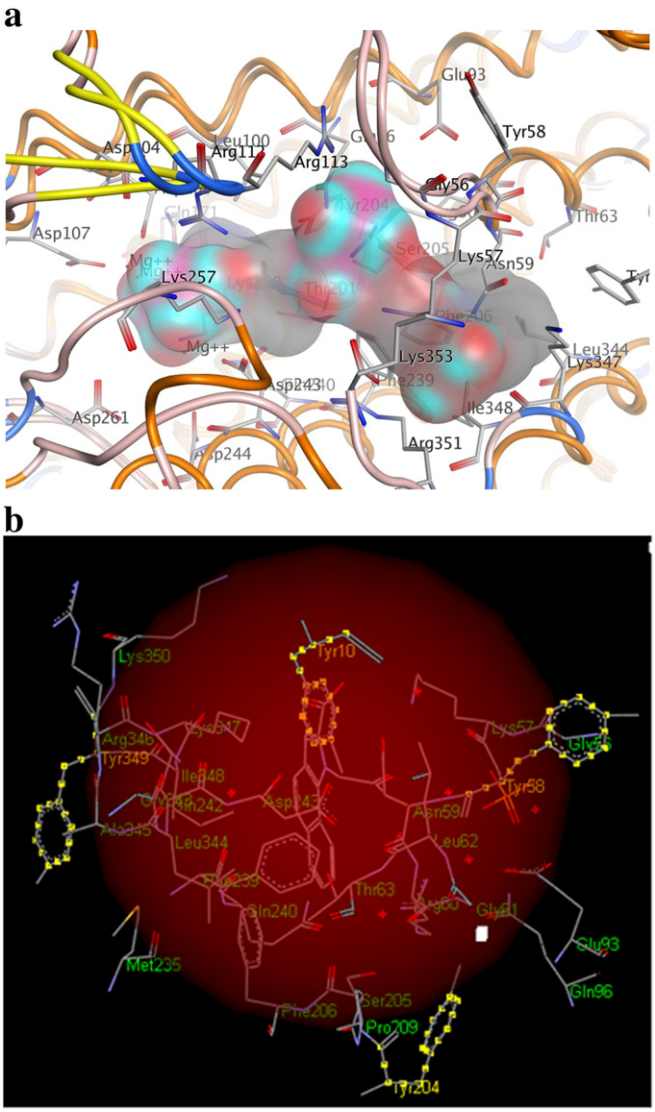

Fig. 2. (a) The substrate binding sites and the allosteric binding site of FPPS. The left pocket is the DMAPP or GPP binding site, the middle pocket is the IPP binding site, and the right pocket is the allosteric binding site. (b) The computer model of allosteric pocket of rat FPPS. Tyr10, Tyr56, Tyr204, and Tyr349 are located in this allosteric pocket.

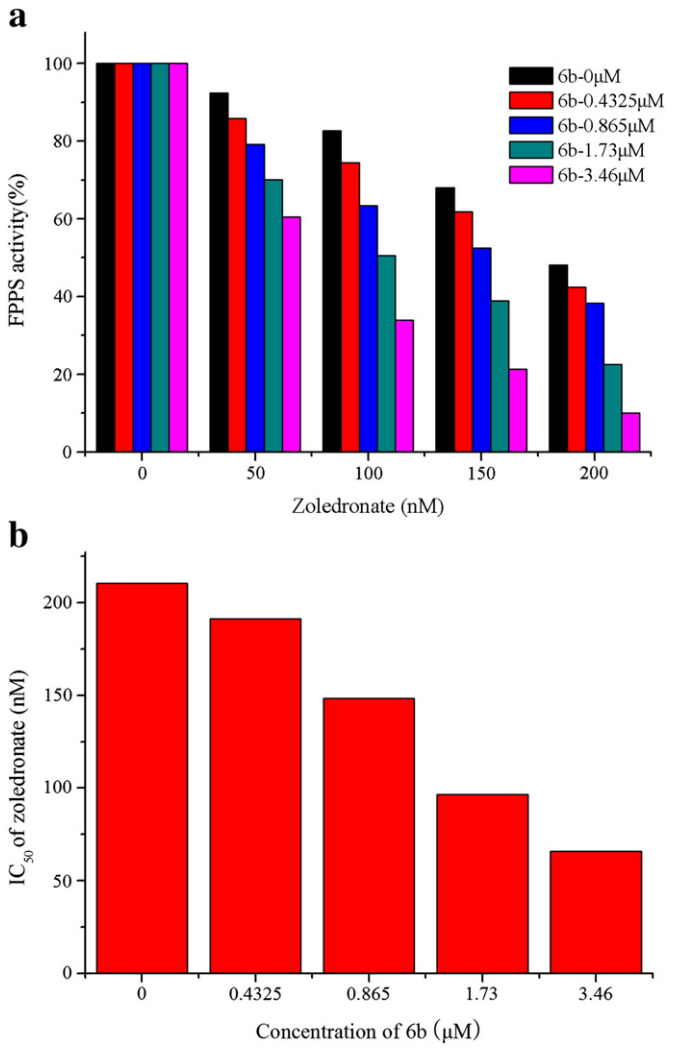

Fig. 4. (a) FPPS activity in the presence of zoledronate and compound **6b**. (b) The IC_{50} of zoledronate in the presence of varying concentration of **6b**. FPPS was incubated with zoledronate alone or with varying concentrations of compound **6b**. The concentrations of zoledronate were 50 nM, 100 nM, 150 nM, and 200 nM, and the concentrations of compound **6b** used were 0.4325 μM, 0.865 μM, 1.73 μM, and 3.46 μM.

Prior to the production step, the following protocol was applied, using SANDER module in AMBER. The solutes were fixed, and the solvent molecules with counter ions were allowed to move during a 2000-step minimization. All the atoms were allowed to be relaxed by a 2000-step full minimization. After the minimization, each complex was gradually heated from 0 to 300 K in 200 ps with solutes

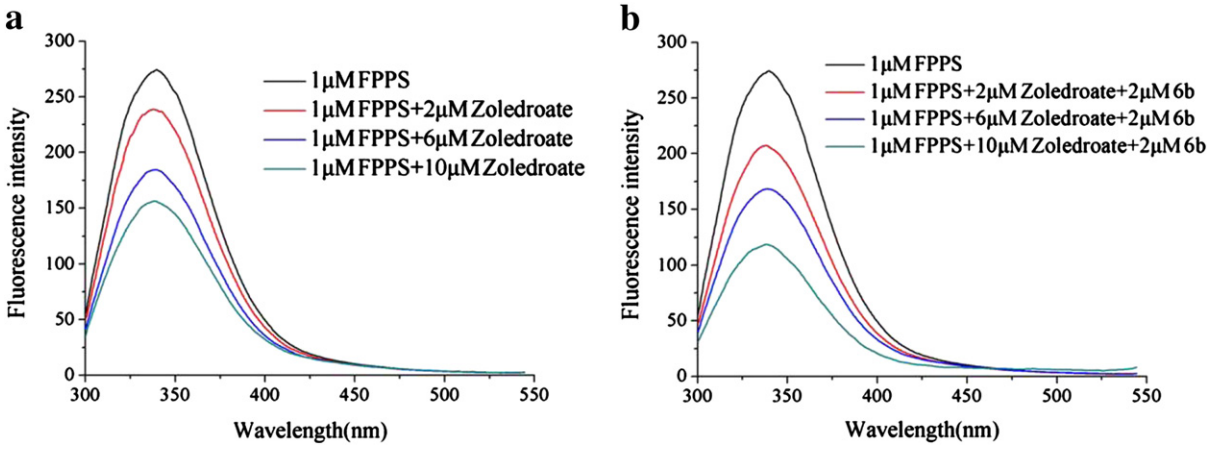

Fig. 3. (a) Fluorescence titration of FPPS with zoledronate in the absence of **6b**. (b) Fluorescence titration of FPPS with zoledronate in the presence of **6b**. The FPPS used was 1 μM, and the zoledronate used was 2 μM, 6 μM, 10 μM in the absence or presence of 2 μM **6b**.

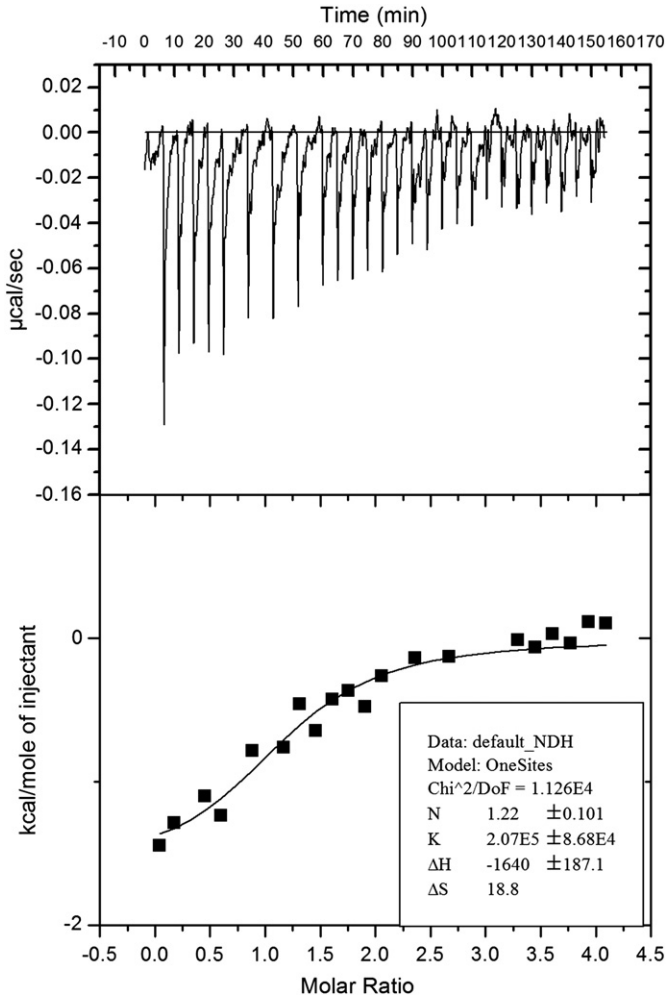

Fig. 5. FPPS was titrated with **6b** in ITC measurement. The data were analyzed to determine binding stoichiometry (N), binding affinity (K_a), and thermodynamic parameters of the reaction using Origin software (OriginLab 7.0).

constrained at a weak harmonic constraint of 5 kcal mol^{-1} $Å^{-2}$. Finally, periodic boundary dynamics simulations of 30 ns were carried out with an NPT (constant composition, pressure, and temperature) ensemble at 1 atm and 300 K in the production step, using GPU accelerated PMEMD in AMBER 12. The temperature was kept at 300 K by means of the weak-coupling algorithm. The SHAKE algorithm was used to fix all covalent bonds containing hydrogen atoms with a time step of 2 fs. The particle-mesh Ewald (PME) method was performed to treat long-range electrostatic interactions. A residue-based cutoff of 10 Å was utilized for the non-covalent interactions.

The MM/PBSA method implemented in the AMBER 12 suite was used to calculate the binding free energy between the receptor and the ligand. The snapshots of last 10 ns from MD trajectories were collected to calculate the binding free energies. The trajectory with a best binding free energy was selected and its conformations were clustered into 3 clusters. The representative conformation from the major cluster was selected for binding mode analysis. The root mean square deviations (RMSD) were calculated and plotted as time series for the receptor backbone and the ligand, respectively.

2.9. MTT assay and fluorescence imaging assay

The types of tumor cells used in the present study included human hepatocellular carcinoma cells (HepG2), human lung carcinoma cell line (NCI), human cervical carcinoma cells (Hela), human leukemia cells (A549 and HL60), and human normal epithelial cells (ECV-304). The cells were seeded on 96-well plates (1.0×10^3/well), and exposed to various concentrations of compounds. After 48 h of treatment at 37 °C in a humidified atmosphere of 5% CO_2, the cells were centrifuged and 10 mL of 5 mg/mL methyl thiazolyl tetrazolium (MTT) solution was added to each well, and incubation was continued for another 4 h. The cells in each well were then treated with dimethyl sulfoxide (DMSO) (200 µL for each well), and the optical density (OD) was recorded at 570 nm. All compound doses were parallel tested in triplicate and the highest dose was 100 µM, and the IC_{50} values were derived from the mean OD values of the triplicate tests versus compound concentrations.

3. Results and discussion

3.1. Organic syntheses of quinoline derivatives

The syntheses of the quinoline derivatives were as follow: the starting materials aniline or 1-naphthylamine and ethyl acetoacetate or ethyl 4-chloroacetoacetate were used to synthesize the intermediates as described previously [28]. These intermediates were reacted with the aromatic esters or aliphatic esters to give the quinoline esters.

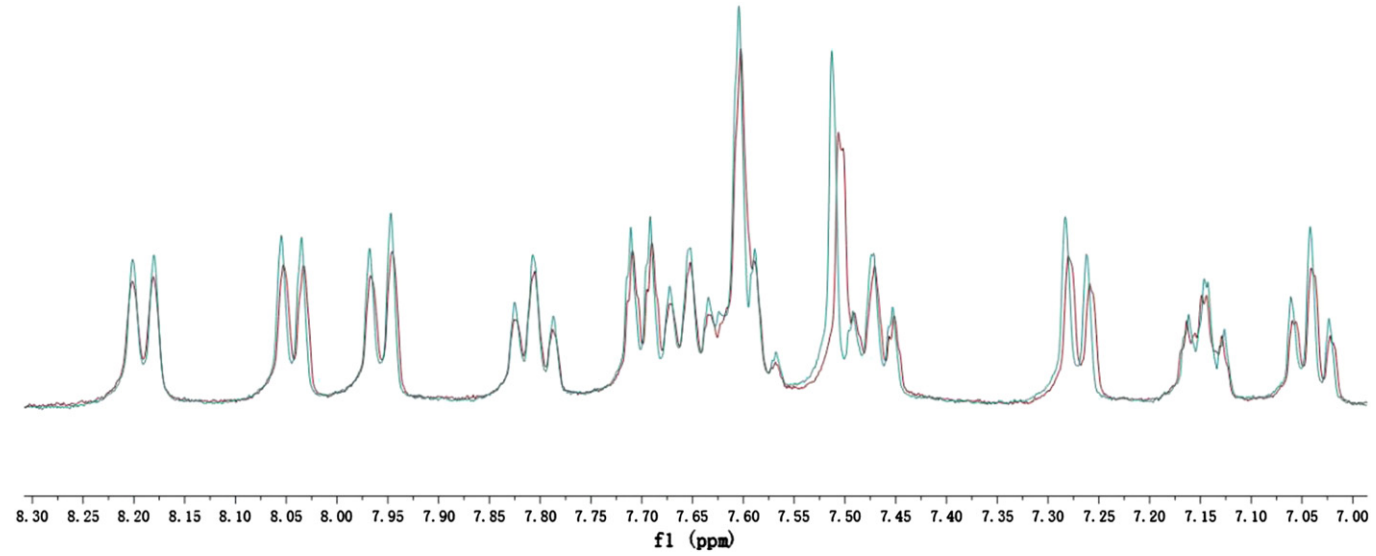

Fig. 6. In vitro HAP experiment for the binding of FPPS with **6b**. FPPS was incubated with **6b** in the presence or absence of 2.0 mg HAP for 5 min, centrifuged, and measured by using NMR.

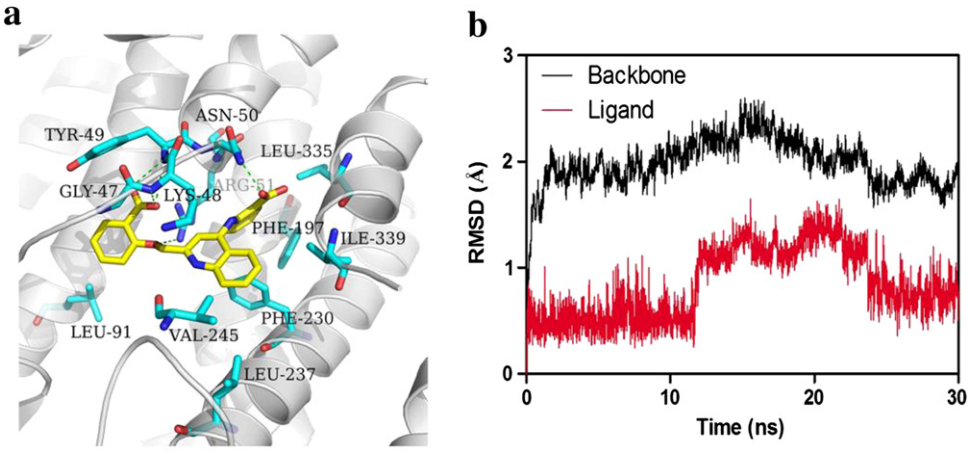

Fig. 7. Molecular modeling study for the interaction between FPPS and **6b**. (a) The binding mode of FPPS with **6b**. (b) The RMSD in the presence and absence of **6b**.

These esters were hydrolyzed with LiOH to generate the acid products. The structures of the lead compounds were validated by using ^{1}H NMR, ^{13}C NMR, and HRMS. The quinoline esters and quinoline acids were then used for the enzyme inhibition studies.

3.2. The enzyme inhibition studies

The designed quinoline esters and acids were incubated with FPPS, assayed with our non-radioactive method [20], and zoledronic acid was used as a control. As shown in Table 1, all these synthetic compounds showed good inhibitory activity against FPPS with their IC_{50} values ranging from 3.46 μM to 28.6 μM. Generally, the acid derivatives showed higher inhibitory effect than their ester derivatives. It is possible that the hydrogen bonding interactions or ionic interactions of the carboxylic acid made strong contribution to the binding. The aromatic core could have hydrophobic interactions and/or π–π stacking interactions with surrounding amino acids in the binding pocket of FPPS. Compounds **6b** and **7a** displayed good inhibitory activity with their IC_{50} values of 3.46 μM and 3.51 μM, respectively.

3.3. Fluorescence titration studies

In order to further confirm the binding between the FPPS and our synthetic compounds, fluorescence titration experiment was performed. Rat FPPS has some tyrosines and tryptophans with aromatic side chains, which let the enzyme have fluorescence [29–31]. Based on the amino acid sequence (Fig. 1) and the computer model of three important binding pockets of rat FPPS (Fig. 2a and b), we found that several residues including Tyr10, Tyr56, Tyr204, and Tyr349 are located around the allosteric site. The binding of small molecule to the enzyme may change hydrophilic and hydrophobic environment around these amino acids, resulting in fluorescence absorbance changes. The fluorescence titration experiment was carried out following that described with minor modification [8,32]. The zoledronate was used as a control. The dissociation constant K_d values (Table 1) were obtained through data fitting using nonlinear regression analysis with equation $Y = [F_{max}(X)] / [K_d + (X)]$. Our result confirmed the binding interactions between the FPPS and our synthetic molecules. The combination of zoledronate and **6b** decreased the fluorescence absorbance of FPPS compared to that with zoledronate alone (Fig. 3). The K_d value for inhibition of FPPS with zoledronate alone was 9.0 μM, and it was decreased to 7.2 μM in the presence of 2 μM **6b**. Similarly, the K_d value for **6b** was 5.78 μM, and it was decreased to 4.84 μM in the presence of 2 μM zoledronate. It should be noted that the calculated K_d values are related with hydrophilic and hydrophobic environmental changes of the surrounding aromatic residues, while IC_{50} values indicated inhibitory effects. Therefore, they are not necessarily correlated, but both support the good binding interactions between the FPPS and our synthetic molecules.

3.4. The studies for the combination of quinoline derivative and zoledronate

To investigate the combination effects of our synthetic compounds with FPPS active-site inhibitor zoledronate, the FPPS was incubated with zoledronate alone or with varying concentrations of compound **6b**. Zoledronate alone gave a dose-dependent inhibition of FPPS with IC_{50} value of ~200 nM, and the addition of compound **6b** apparently accelerated this inhibition (Fig. 4a), especially the combination of 3.46 μM **6b** and 200 nM zoledronate had nearly 90% inhibition of FPPS, indicating the possibility for the combined use of these two inhibitors. The IC_{50} value of zoledronate decreased from 200 nM to 66 nM in the presence of **6b** (Fig. 4b). Then, the CompuSyn software was used to calculate the CI value (Supporting Information). The CI values for the combinations of low concentrations of zoledronate (50 nM, 100 nM, 150 nM) with various concentrations of **6b** (0.4325 μM, 0.865 μM, 1.73 μM, 3.46 μM) were approximately 1, indicating the possibility of the additive effect or antagonism. The combinations of 200 nM zoledronate and various concentrations of **6b** had the CI values of less than 1, indicating the possibility of the synergism. However, the real effect for the combination use of these two inhibitors may be more thoroughly evaluated through long term

Table 2
The cytotoxic effects of the quinoline derivatives on cancer cells.

Compound	IC_{50} (μM)					
	HepG2	NCI	Hela	HL60	A549	ECV304
4a	28.6	37.9	31.8	20.2	29.9	26.0
4b	30.2	44.6	50.1	44.2	18.4	70.8
5a	93.8	78.7	70.3	36.6	67.4	>100
5b	25.9	37.2	73.2	30.6	41.1	60.6
6a	45.8	54.5	50.0	12.2	15.8	99.7
6b	26.2	36.3	20.5	16.4	17.4	70.7
7a	49.6	50.4	35.7	19.4	27.4	>100
7b	49.6	92.8	77.3	80.3	76.8	>100
8a	52.1	27.8	36.6	31.1	16.8	>100
8b	85.8	82.8	75.3	37.6	43.3	>100
9a	65.6	90.2	57.5	56.8	73.5	>100
9b	28.8	47.5	30.2	20.7	65.3	>100
10a	18.6	28.3	25.0	7.16	24.3	65.3
10b	58.4	62.6	33.0	44.4	83.6	>100
11a	23.3	27.2	29.1	8.09	33.2	>100
11b	16.6	65.1	47.7	25.6	78.7	>100
12a	60.3	66.8	38.8	15.8	20.2	>100
12b	85.8	82.2	73.6	43.2	25.8	>100
13a	40.0	84.4	20.2	17.6	72.1	>100
13b	96.2	45.5	80.6	34.5	67.4	>100

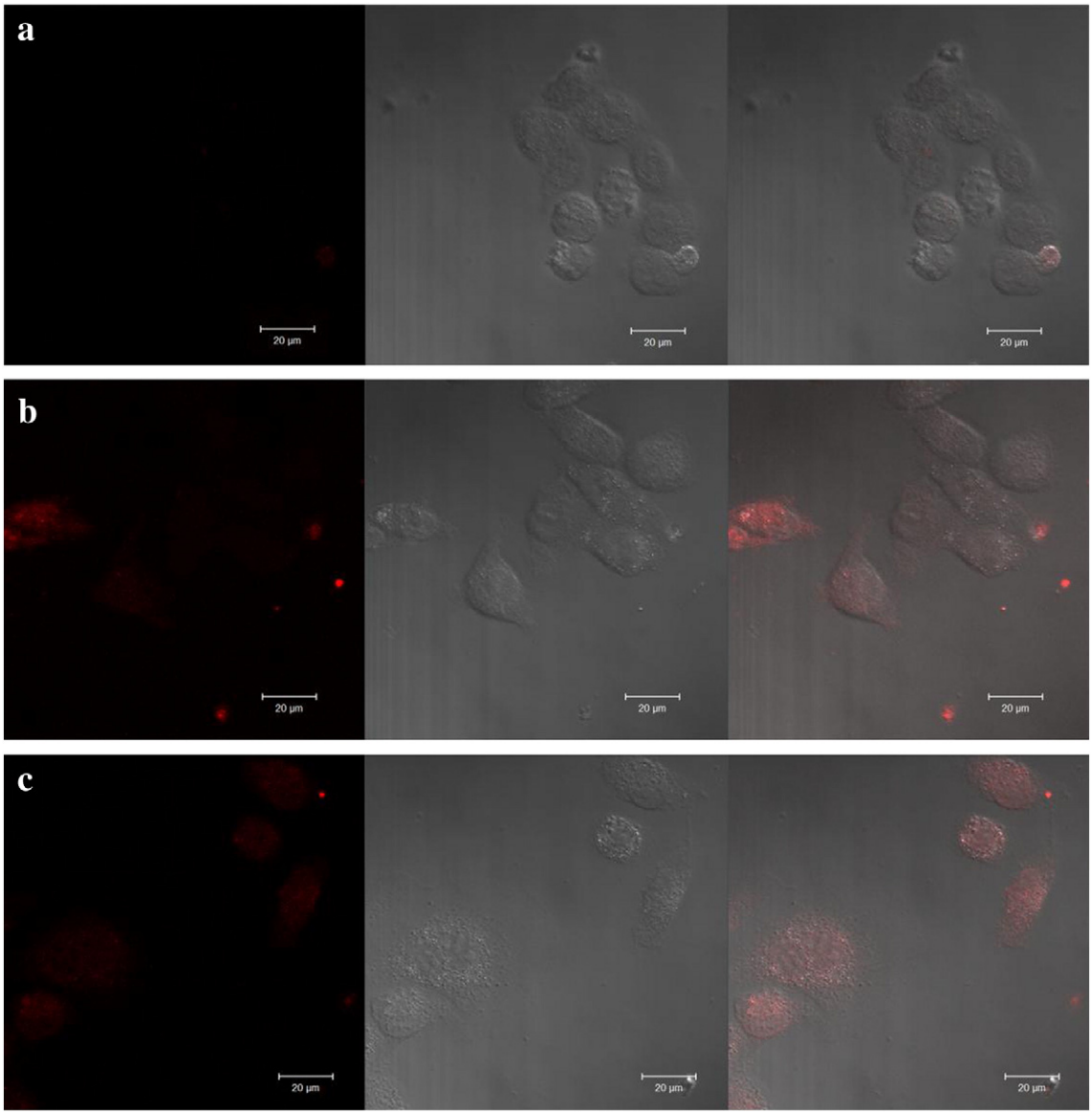

Fig. 8. Uptake of **6a** and **6b** by human Hela cells. Cells were incubated with compound **6a** or **6b** (10 μM) for 6 h, and were subsequently examined via fluorescent microscopy. Control cells under phase-contrast microscopy and under fluorescent microscopy are also shown. (a) Hela cells were treated with DMSO for 6 h; (b) Hela cells were treated with **6a** for 6 h; (c) Hela cells were treated with **6b** for 6 h.

monitoring their injection in animal experiments in the future. Although the IC_{50} value of compound **6b** (3.46 μM) is ~17 times higher than that of zoledronate, considering tumor cell permeability problem of zoledronate, the combined use of these two types of compounds might be more effective for cancer treatment.

3.5. ITC study for the binding of quinoline derivatives with FPPS

In order to gain insight details on the binding affinity and the binding ratio of quinoline derivatives for FPPS, ITC experiment was performed to characterize the energy of molecular binding interactions [33–35]. The titration of FPPS with compound **6b** was carried out, with FPPS and **6b** both dissolved in the same dialysis buffer. The titration results including corresponding enthalpy values are shown in Fig. 5, and small aliquots of **6b** solution were added from the syringe into the microcalorimeter cells containing FPPS. The ligand dilution control experiment was also carried out, and the same **6b** solution was added from the syringe into the dialysis buffer without FPPS in the cell. We found that the enthalpy change for ligand dilution was typically quite small in magnitude. The resulting net enthalpy change was then determined by subtracting the value of dilution control. From Fig. 5, we determined a binding stoichiometry of approximately 1:1 for the binding of **6b** to one subunit of the FPPS homodimer. The binding of **6b** to FPPS was found to be exothermic, and the binding enthalpy and entropy in this entropy-driven binding event were determined to be -1.64 kcal mol^{-1} and 18.8 cal mol^{-1} K^{-1}, respectively. The resulting K_d value was determined to be 4.8 μM, which is consistent with the measured IC_{50} value (3.46 μM) with the enzymatic assay. The free energy (ΔG) was determined to be -7.25 kcal mol^{-1}, indicating that the binding of **6b** to FPPS is exothermic.

3.6. NMR-based HAP binding assay

The traditional bisphosphonate compounds show strong binding to hydroxyapatite (HAP) that is the major mineral component of bone, making it less available for membrane penetration into tumor cells [36]. In our experiment, the binding of quinoline derivatives to HAP was determined by using ^1H NMR. After the addition of 2.0 mg HAP,

the ^{1}H NMR signal (cyan line) was almost the same as that for the **6b** alone (dark red line), as shown in Fig. 6. This result showed that the compound **6b** had almost no binding with bone material, which should be more available for membrane penetration into tumor cells.

3.7. Molecular modeling study

To investigate the interacting mode between our synthetic compounds and FPPS (PDB code: 3N6K), a molecular modeling study utilizing the docking program named AUTODOCK 4.0 package with Discovery Studio 2.5 was carried out [37]. As shown in Fig. 7a, compound **6b** can well occupy the allosteric pocket of FPPS. The carboxylate groups connected with two benzene rings show strong hydrogen-bonding interactions with Tyr49, Gly47, Lys48 and Asn50, and Lys48 also has electrostatic interaction with the carboxylate group of **6b**. The oxygen atom located in the salicylic acid phenolic hydroxyl group also has the similar hydrogen-bonding interaction with Lys48, improving the binding affinity of **6b** to this pocket. The quinoline core penetrates deeply into the pocket, and the introduction of benzene ring contributes π–π stacking interactions with Phe197 and Phe230, and hydrophobic interactions with Tyr49, Gly47 and Lys48.

The root mean square deviations (RMSD) were calculated and plotted as time series for the receptor backbone and the ligand, respectively, as shown in Fig. 7b. The backbone RMSD of FPPS reached 2 Å within a short time and stayed relatively stable during the whole 30 ns simulation, indicating a global equilibrium state. The ligand **6b** RMSD was stable for the first 10 ns and increased to 2 Å afterwards, then slightly declined. The trend of ligand RMSD is in good agreement with that of the receptor, which may imply a good ligand-induced fit of receptor.

3.8. Cytotoxic effects on cancer cells and cell localization

MTT assays were performed to evaluate the cytotoxic effects of the quinoline derivatives on cancer cells. Most compounds showed mild cytotoxic effects to cancer cells, and the best inhibition activity was found for compounds **10a** and **11a** with their IC_{50} values of 7.16 μM and 8.09 μM for HL60 cells. The IC_{50} value of **6b** ranged from 16.4 μM to 36.3 μM for different cancer cells. These quinoline derivatives showed nearly no cytotoxic effects to human normal vascular endothelial cell ECV304, with their IC_{50} values mostly more than 100 μM (Table 2).

Fluorescence imaging is a very important technique for biological studies and clinical applications due to high temporal and spatial resolutions. In the present study, fluorescent microscopy was performed to assess the cellular uptake of the fluorescent compounds **6b** and **6a**. Hela cells were incubated with compound **6b** or **6a** (10 μM) for 6 h, and were subsequently examined via confocal fluorescent microscopy. As shown in Fig. 8, the fluorescence microscopy clearly showed that compounds **6b** and **6a** can penetrate Hela cells.

In summary, we designed and synthesized a series of non-bisphosphonate quinoline derivatives, which were found to be new FPPS inhibitors. Molecular modeling and ITC studies indicated that compound **6b** can well occupy the allosteric pocket of FPPS with a 1:1 binding stoichiometry. None of these compounds showed measurable affinity to hydroxyapatite, indicating their low affinity to bone mineral material. Compound **6b** showed synergistic effect with zoledronate for FPPS inhibition, indicating the possibility for the combined use of these two inhibitors. Compound **6b** could become a lead compound for further development for the treatment of cancer.

Acknowledgements

We thank Sun Yat-sen University and the National Natural Science Foundation of China (Grant 21242010) for the financial support of this study.

Appendix A. Supplementary data

The CompuSyn software calculation of the CI value. This information can be found in the online version at http://dx.doi.org/10.1016/j.bbagen.2013.11.006.

References

[1] R. Russell, P. Croucher, M. Rogers, Bisphosphonates: pharmacology, mechanisms of action and clinical uses, Osteoporos. Int. 9 (1999) S66–S80.
[2] R.E. Coleman, The role of bisphosphonates in breast cancer, Breast 13 (Suppl. 1) (2004) S19–S28.
[3] S. Sun, C.E. McKenna, Farnesyl pyrophosphate synthase modulators: a patent review (2006–2010), Expert. Opin. Ther. Pat. 21 (2011) 1433–1451.
[4] R.G.G. Russell, Bisphosphonates: from bench to bedside, Ann. N. Y. Acad. Sci. 1068 (2006) 367–401.
[5] B.M. Wasko, A. Dudakovic, R.J. Hohl, Bisphosphonates induce autophagy by depleting geranylgeranyl diphosphate, J. Pharmacol. Exp. Ther. 337 (2011) 540–546.
[6] J.R. Green, Bisphosphonates: preclinical review, Oncologist 9 (2004) 3–13.
[7] M.J. Rogers, S. Gordon, H. Benford, F. Coxon, S. Luckman, J. Monkkonen, J. Frith, Cellular and molecular mechanisms of action of bisphosphonates, Cancer 88 (2000) 2961–2978.
[8] P. Dürrschmidt, J. Mansfeld, R. Ulbrich-Hofmann, Differentiation between conformational and autoproteolytic stability of the neutral protease from *Bacillus stearothermophilus* containing an engineered disulfide bond, Eur. J. Biochem. 268 (2001) 3612–3618.
[9] M.J. Fischer, S. Meyer, P. Claudel, M. Bergdoll, F. Karst, Identification of a lysine residue important for the catalytic activity of yeast farnesyl diphosphate synthase, Protein J. 30 (2011) 334–339.
[10] K.L. Kavanagh, K. Guo, J.E. Dunford, X. Wu, S. Knapp, F.H. Ebetino, M.J. Rogers, R.G.G. Russell, U. Oppermann, The molecular mechanism of nitrogen-containing bisphosphonates as antiosteoporosis drugs, Proc. Natl. Acad. Sci. 103 (2006) 7829–7834.
[11] R.G.G. Russell, Z. Xia, J.E. Dunford, U. Oppermann, A. Kwaasi, P.A. Hulley, K.L. Kavanagh, J.T. Triffitt, M.W. Lundy, R.J. Phipps, Bisphosphonates, Ann. N. Y. Acad. Sci. 1117 (2007) 209–257.
[12] C.M. Shipman, M.J. Rogers, J.F. Apperley, R.G.G. Russell, P.I. Croucher, Bisphosphonates induce apoptosis in human myeloma cell lines: a novel anti-tumour activity, Br. J. Haematol. 98 (1997) 665–672.
[13] V. Stresing, F. Daubiné, I. Benzaid, H. Mönkkönen, P. Clézardin, Bisphosphonates in cancer therapy, Cancer Lett. 257 (2007) 16–35.
[14] D. Glick, S. Barth, K.F. Macleod, Autophagy: cellular and molecular mechanisms, J. Pathol. 221 (2010) 3–12.
[15] Y. Zhang, R. Cao, F. Yin, M.P. Hudock, R.-T. Guo, K. Krysiak, S. Mukherjee, Y.-G. Gao, H. Robinson, Y. Song, J.H. No, K. Bergan, A. Leon, L. Cass, A. Goddard, T.-K. Chang, F.-Y. Lin, E.V. Beek, S. Papapoulos, A.H.J. Wang, T. Kubo, M. Ochi, D. Mukkamala, E. Oldfield, Lipophilic bisphosphonates as dual farnesyl/geranylgeranyl diphosphate synthase inhibitors: an X-ray and NMR investigation, J. Am. Chem. Soc. 131 (2009) 5153–5162.
[16] P.G. Fournier, F. Daubine, M.W. Lundy, M.J. Rogers, F.H. Ebetino, P. Clezardin, Lowering bone mineral affinity of bisphosphonates as a therapeutic strategy to optimize skeletal tumor growth inhibition in vivo, Cancer Res. 68 (2008) 8945–8953.
[17] J.M. Rondeau, F. Bitsch, E. Bourgier, M. Geiser, R. Hemmig, M. Kroemer, S. Lehmann, P. Ramage, S. Rieffel, A. Strauss, J.R. Green, W. Jahnke, Structural basis for the exceptional in vivo efficacy of bisphosphonate drugs, ChemMedChem 1 (2006) 267–273.
[18] R. Cao, C.K. Chen, R.T. Guo, A.H. Wang, E. Oldfield, Structures of a potent phenylalkyl bisphosphonate inhibitor bound to farnesyl and geranylgeranyl diphosphate synthases, Proteins 73 (2008) 431–439.
[19] M.S. Marma, Z. Xia, C. Stewart, F. Coxon, J.E. Dunford, Synthesis and biological evaluation of r -halogenated bisphosphonate and phosphonocarboxylate analogues of risedronate, J. Med. Chem. 50 (2007) 9.
[20] J. Gao, X. Chu, Y. Qiu, L. Wu, Y. Qiao, J. Wu, D. Li, Discovery of potent inhibitor for farnesyl pyrophosphate synthase in the mevalonate pathway, Chem. Commun. (Camb.) 46 (2010) 5340–5342.
[21] J. Gao, J. Liu, Y. Qiu, X. Chu, Y. Qiao, D. Li, Multi-target-directed design, syntheses, and characterization of fluorescent bisphosphonate derivatives as multifunctional enzyme inhibitors in mevalonate pathway, Biochim. Biophys. Acta Gen. Subj. 1830 (2013) 3635–3642.
[22] W. Jahnke, J.-M. Rondeau, S. Cotesta, A. Marzinzik, X. Pellé, M. Geiser, A. Strauss, M. Götte, F. Bitsch, R. Hemmig, C. Henry, S. Lehmann, J.F. Glickman, T.P. Roddy, S.J. Stout, J.R. Green, Allosteric non-bisphosphonate FPPS inhibitors identified by fragment-based discovery, Nat. Chem. Biol. 6 (2010) 660–666.
[23] L. Lengyel, T.Z. Nagy, G. Sipos, R. Jones, G. Dormán, L. Ürge, F. Darvas, Highly efficient thermal cyclization reactions of alkylidene esters in continuous flow to give aromatic/heteroaromatic derivatives, Tetrahedron Lett. 53 (2012) 738–743.
[24] R.M. Gengan, P. Pandian, C. Kumarsamy, P.S. Mohan, Convenient and Efficient microwave-assisted synthesis of a methyl derivative of the fused indoloquinoline alkaloid cryptosanguinolentine, Molecules 15 (2010) 3171–3178.
[25] A. Avetisyan, I. Aleksanyan, L. Ambartsumyan, Synthesis of 6, 8-substituted 4-(hydroxyphenylamino)-and 4-(aminophenylamino)-2-methylquinolines, Russ. J. Org. Chem. 43 (2007) 1048–1051.
[26] T.C. Chou, Theoretical basis, experimental design, and computerized simulation of synergism and antagonism in drug combination studies, Pharmacol. Rev. 58 (2006) 621–681.

[27] T.C. Chou, Drug combination studies and their synergy quantification using the Chou–Talalay method, Cancer Res. 70 (2010) 440–446.
[28] Z.-Q. Liu, S.-T. Zhuo, J.-H. Tan, T.-M. Ou, D. Li, L.-Q. Gu, Z.-S. Huang, Facile syntheses of disubstituted bis(vinylquinolinium)benzene derivatives as G-quadruplex DNA binders, Tetrahedron 69 (2013) 4922–4932.
[29] F.H. Ebetino, A.M. Hogan, S. Sun, M.K. Tsoumpra, X. Duan, J.T. Triffitt, A.A. Kwaasi, J.E. Dunford, B.L. Barnett, U. Oppermann, M.W. Lundy, A. Boyde, B.A. Kashemirov, C.E. McKenna, R.G. Russell, The relationship between the chemistry and biological activity of the bisphosphonates, Bone 49 (2011) 20–33.
[30] K. Ohno, K. Mori, M. Orita, M.T., Computational Insights into Binding of Bisphosphates to Farnesyl Pyrophosphate Synthase Current Medicinal Chemistry, 18 (2011) 220–233.
[31] X. Chu, W. Yu, L. Wu, X. Liu, N. Li, D. Li, Effect of a disulfide bond on mevalonate kinase, Biochim. Biophys. Acta 1774 (2007) 1571–1581.
[32] M.L. Colgrave, D.J. Craik, Thermal, chemical, and enzymatic stability of the cyclotide kalata B1: the importance of the cyclic cystine knot†, Biochemistry 43 (2004) 5965–5975.
[33] M.L. Doyle, Characterization of binding interactions by isothermal titration calorimetry, Curr. Opin. Biotechnol. 8 (1997) 31–35.
[34] B. Pagano, C. Giancola, Energetics of quadruplex-drug recognition in anticancer therapy, Curr. Cancer Drug Targets 7 (2007) 520–540.
[35] B. Pagano, C.A. Mattia, C. Giancola, Applications of isothermal titration calorimetry in biophysical studies of G-quadruplexes, Int. J. Mol. Sci. 10 (2009) 2935–2957.
[36] W. Jahnke, C. Henry, An in vitro assay to measure targeted drug delivery to bone mineral, ChemMedChem 5 (2010) 770–776.
[37] G.M. Morris, D.S. Goodsell, R.S. Halliday, R. Huey, W.E. Hart, R.K. Belew, A.J. Olson, Automated docking using a Lamarckian genetic algorithm and an empirical binding free energy function, J. Comput. Chem. 19 (1998) 1639–1662.